Uptake and desorption of hydrophilic compounds from human stratum corneum

Matthew A. Miller, Fang Yu, Keun-il Kim, Gerald B. Kasting

PII: S0168-3659(17)30679-X
DOI: doi: 10.1016/j.jconrel.2017.06.015
Reference: COREL 8838

To appear in: *Journal of Controlled Release*

Received date: 17 December 2016
Revised date: 2 June 2017
Accepted date: 17 June 2017

Please cite this article as: Matthew A. Miller, Fang Yu, Keun-il Kim, Gerald B. Kasting , Uptake and desorption of hydrophilic compounds from human stratum corneum. The address for the corresponding author was captured as affiliation for all authors. Please check if appropriate. Corel(2017), doi: 10.1016/j.jconrel.2017.06.015

Uptake and Desorption of Hydrophilic Compounds from Human Stratum Corneum

Matthew A. Miller[†], Fang Yu[‡], Keun-il Kim[†‡] and Gerald B. Kasting[†*]

[†]The James L. Winkle College of Pharmacy
The University of Cincinnati

[‡]College of Engineering and Applied Science,
The University of Cincinnati

[†‡]College of Arts & Sciences, Dept. of Chemistry
The University of Cincinnati

[*]Correspondence:

Gerald B. Kasting
The University of Cincinnati Academic Health Center
P.O. Box 670514
Cincinnati, Ohio 45267-0514

Phone: (513) 558-1817
Fax: (513) 558-0978
Email: Gerald.Kasting@uc.edu

Abstract

Small, polar compounds, both ionic and uncharged, partition into human stratum corneum immersed in aqueous solutions to an extent comparable to the water volume fraction of the tissue, then desorb in two phases. The fast phase has a time constant on the order of a few minutes, whereas the slow phase occurs over many hours. A physical model for this behavior involving a combination of tranverse diffusion through the tissue and lateral diffusion and exchange with skin appendages is presented. This concept is probed using excised human stratum corneum exposed to aqueous solutions of radiolabeled sodium chloride, tetraethyl ammonium bromide and mannitol, plus previously published data on six other compounds of varying molecular size and polarity. The fast phase desorption process becomes unimportant for lipophilic compounds. Slow phase desorption rates are size-selective, with larger species desorbing much more slowly than smaller ones. Interpreting the size-selectivity in terms of smooth cylindrical pores using the centerline approximation leads to an optimum pore radius of about 8-12 Å, depending on the model chosen.

Keywords: Desorption, Diffusion, Mathematical model, Skin, Stratum corneum, Transport

Chemical compounds studied in this article:

Glycerin (PubChem CID:753)
D-Mannitol (PubChem CID:6251)
Niacinamide (PubChem CID:936)
1-Propanol (PubChem CID:1031)
Sodium chloride (PubChem CID:5234)
Sucrose (PubChem CID:5988)
Testosterone (PubChem CID:6013)
Tetraethylammonium bromide (PubChem CID:6285)
Water (PubChem CID:962)

1. Introduction

The skin's outermost layer, the stratum corneum (SC), forms a very effective barrier for polar solutes including water, sugars and salts; this is an essential, life-preserving function of the tissue. The diffusion barrier is thought by most to arise primarily from the highly ordered, gel phase bilayer lipids secreted into the intercellular spaces during terminal differentiation of the epidermal keratinocytes [1]. Small amounts of polar solutes can and do penetrate the SC, as shown by its conductivity under low constant electric fields [2-4] and numerous in vitro permeation experiments, for example [5-7]. The extent to which large hydrophilic solutes can penetrate the SC without some perturbation to the barrier is still a matter of debate, although it must be small considering how much work has gone into making this happen at therapeutic drug levels [8, 9].

It is fair to say that Mitragotri's 2003 analysis [10] is the most widely recognized model of how hydrophilic solutes enter the skin, although other noteworthy examples exist [4, 11, 12]. Mitragotri proposed four diffusion pathways through skin, two of which applied to lipophilic compounds, the other two to hydrophilic compounds. Of the models cited, only Chen et al. [12] consider that hydrophilic solutes enter corneocytes within the SC; the others consider porous networks within the lipids [10, 11], non specific transport in appendages [10] or else are silent on this issue [4].

In considering this problem we found that there was little available information on the *amounts* of hydrophilic permeants in the SC, and the rates at which they entered and desorbed from the tissue. Surely such information could help to distinguish between intercellular, transcellular and appendageal transport routes. Consequently we designed a study to develop this information, using established uptake and desorption methods for radiolabeled solutes placed in contact with isolated

human SC [13-15]. Some data were already available from earlier work in our laboratories [15-17]. To this database we have added studies on three inorganic salts – ^{22}NaCl, Na^{36}Cl and ^{14}C-tetraethylammonium bromide (^{14}C-TEAB) – and one sugar alcohol, ^{14}C-mannitol. Results are analyzed in terms of a two-phase model involving rapid and slow desorption processes. They are discussed in terms of the Mitragotri (2003) model [10] and also an appendageal model for transport of hydrophilic compounds currently under consideration in our laboratory [18, 19], an analytical approximation to which is presented here.

Desorption kinetics of water from human SC [20, 21] and of both lipophilic and moderately hydrophilic compounds from powdered bovine hoof/horn keratin [22] have been analyzed by others in terms of slowly reversible binding of the permeants to keratin, as has the SC permeation profile of theophylline, another moderately hydrophilic compound [23]. It was of interest to examine whether slowly reversible binding to keratin or other SC proteins could explain the desorption profiles observed in this study. Comments on this analysis are offered later.

2. Experimental

2.1. Materials

Excised split thickness human cadaver skin from the posterior leg (3 donors for each treatment) having a nominal thickness of 400 μm, was procured from The New York Firefighters Skin Bank. The skin was preserved in RPMI 1640 (ThermoFisher Scientific, Waltham, MA) with 10% glycerol, oxacillin sodium and gentamicin and kept at −80ºC until use. Sodium chloride, [^{22}Na] (4524.3 mCi/mmol; 0.1 mCi/mL) and tetraethylammonium bromide [^{14}C-TEAB] (3.5 mCi/mmol, 0.1 mCi/mL) were purchased from Perkin Elmer (Shelton, CT). Sodium chloride, [^{36}Cl] (16 mCi / mgCl; 0.1 mCi/mL) and mannitol, D-[1-^{14}C]- (55 mCi/mmol, 0.1 mCi/mL; 2:98

ethanol/water) were purchased from American Radiolabeled Chemicals (St. Louis, MO). The supplier stated that the radiochemical purity of the ^{14}C-mannitol was greater than or equal to 99%. Unlabelled sodium chloride, tetraethylammonium bromide and D-mannitol, each at least 98% pure, were purchased from Fisher Scientific (Pittsburgh, PA). Calcium-free Dulbecco's phosphate-buffered saline was obtained from Sigma-Aldrich. Solvable™ (a tissue solubilizer) was purchased from Perkin-Elmer (Shelton, CT).

2.2. Hydrodynamic radii calculations

Hydrodynamic radii, r_{se}, for ionic solutes (Na^+, Cl^- and TEA^+) were calculated from the Stokes-Einstein relationship using ionic mobility data from the literature [24]. The value for water, r_{se} = 1.1 Å, was calculated in the same manner using a water self-diffusivity value of 2.44×10^{-5} cm^2/s at 25°C [25]. Hydrodynamic radii for the remaining solutes were calculated in a similar manner, but using Wilke-Chang estimates for aqueous diffusivity as described in [26] [(cf. their Eq. (1)].

2.3. Uptake/desorption studies

The method has been described in detail by Talreja [17] and summarized elsewhere [15, 16]. Aqueous solutions of radiolabeled solute – ^{22}NaCl (0.015 μCi/mL), $Na^{36}Cl$ (0.5-0.7 μCi/mL), ^{14}C-TEAB (0.4-4.2 μCi/mL), and ^{14}C-mannitol (2.5 μCi/mL) – were prepared along with sufficient unlabeled solute to yield chemical concentrations of 0.15, 1.5, 15, and 150 mM in 18 MΩ water. Solutions used in the mannitol treatments also contained 0.02% NaN_3 (Fisher Scientific) to inhibit microbial growth. The pH of the NaCl and TEAB solutions was determined prior to adding the radiolabel. Values ranged from 5.6 – 8.2 for the NaCl solutions and 5.9 – 6.4 for the TEAB solutions (see Supplementary Material). Isolated human stratum corneum (HSC) was prepared by

heat separation followed by trypsinization [27], cut into 1.5 cm × 1.5 cm pieces, dried in a desiccator over anhydrous calcium sulfate, and then stored in the dessicator at −20°C until the time of use. On the first day of the experiment, the samples were removed from the dessicator and allowed to equilibrate at ambient temperature and relative humidity (RH) until their weight was constant (~1 h). The ambient weights (m_{amb}) were obtained on an analytical balance. The samples were then rehydrated in water and traced to determine their exact area (A_{wet}). Ambient weights were used to create a randomized block design and an associated concentration assignment. HSC samples were soaked in 0.9–1.2 mL radiolabeled loading solution and equilibrated in an incubator shaker (Innova 400, New Brunswick Scientific) at 32°C and 120 RPM for 3–4 days.

After the equilibration period, HSC samples were removed from vials and quickly rinsed in water. An aliquot of the uptake solution was obtained for later analysis. HSC samples were placed in vials containing 5 mL of their respective desorption solution (chemically equivalent to the uptake solution, but without radiolabel) at 32°C with periodic, vigorous manual shaking to ensure that both sides of the sample were frequently exposed to the solution. After 15 min (the second sampling), the HSC was mounted onto aluminum wire screens, and the assembly was placed in a 7 mL scintillation vial to which 5 mL of temperature-equilibrated desorption solution had been added. The change in procedure at 15 min was dictated by timing constraints. The HSC samples were then maintained in the incubator shaker at 120 RPM to ensure proper temperature and mixing. Subsequent samples were taken by pouring out the liquid contents and replacing with fresh desorption solution. The amount of solution adhering to the tissue sample and screen was considered to be negligible relative to the 5 mL total volume. After the final sampling, 1 mL of Solvable™ (Perkin-Elmer) was added to all HSC samples, which were then maintained at 50°C for at least 3 hours or until the sample was dissolved. The desorption, equilibrium uptake solution

aliquots, and dissolved tissue samples were analyzed for β-decay in Ultima Gold XR™ cocktail using a Tri-Carb 2900TR Liquid Scintillation Analyzer. Results were calculated as disintegrations per minute (DPM) desorbed per cm^2 of hydrated tissue, then converted into μg cm^{-2} using the specific activity of the radiolabeled probe. The sum of all the individual samples from a single piece of skin was designated M^{∞} (μg cm^{-2}). Because sampling times varied slightly, a cubic and/or linear spline was fit to fraction desorbed for each trial and evaluated at common time points so that a mean value could be obtained for each treatment and each approximate sampling time.

2.4. HSC membrane thickness and membrane/vehicle partition coefficient

The membrane thickness is a key parameter in the analysis of desorption data. We initially attempted to measure the weights of equilibrated, fully hydrated HSC samples directly; however, these measurements were imprecise due to water evaporation and possibly also due to inconsistency in removal of excess water from the HSC samples. The mass of the tissue at ambient RH and temperature, m_{amb}, and the hydrated surface area, A_{wet}, were available. In order to estimate the hydrated thickness we made three assumptions: (1) Water sorption in the tissue followed the Guggenheim-Anderson-deBoer (GAB) isotherm described in Li et al. [28]. (2) Ambient RH in the laboratory was comparable to the average outdoor RH. This was supported by a trend toward higher m_{amb}/ A_{wet} ratios in the summer months. (3) Water uptake under fully hydrated conditions was limited to a volume fraction ϕ_{wet} = 0.78, the average value achieved for HSC immersed in normal saline, a_w = 0.996, for 24 h [29]. Although the GAB isotherm predicts even greater water sorption from pure water, a_w = 1.000, the data supporting a higher value for moderate exposure times are limited [30, 31]. Thickness was then calculated as follows:

1. Look up average RH on test day and calculate ambient water activity in HSC sample as a_w^{amb} = RH/100. Choose water activity in fully hydrated HSC to be a_w^{wet} = 0.99575.

2. Calculate water adsorption volume V in HSC membrane under ambient and fully hydrated conditions using GAB isotherm,

$$\frac{V}{V_m} = \frac{cka_w}{(1-ka_w)(1-ka_w+cka_w)} \quad (1)$$

where c = 4.39, k = 0.9901 and V_m = 0.0386 g water/g dry HSC [28].

3. Calculate water volume fraction ϕ in HSC membrane under ambient (ϕ_{amb}) and fully hydrated (ϕ_{wet}) conditions as [31]

$$\phi = \frac{\rho_{mem}V}{\rho_w+\rho_{mem}V} \quad (2)$$

where ρ_{mem} = 1.3 g/cm^3 is the density of dry HSC [32] and ρ_w = 1.0 g/cm^3 is the density of water. For fully hydrated HSC ($a_w = a_w^{wet}$), Eqs. (1) and (2) yield ϕ_{wet} = 0.7800.

4. Calculate the density of HSC at ambient hydration levels as

$$\rho_{amb} = \rho_w\phi_{amb} + \rho_{mem}(1-\phi_{amb}) \quad (3)$$

5. Calculate the thickness of the hydrated HSC membrane as

$$h_{wet} = \frac{m_{amb}(1-\phi_{amb})}{\rho_{amb}A_{wet}(1-\phi_{wet})} \text{ cm.} \quad (4)$$

The derivation of Eq. (4) is given in the Supplementary Material.

For each skin donor, the h_{wet} values for individual samples were averaged to obtain a mean thickness, $\bar{h}_{wet}$. This value was used in the partition coefficient analysis discussed below. Use of the donor average thickness rather than those calculated for the individual samples yielded greater precision in the results, as reflected by smaller standard deviations of the calculated partition coefficients. Values of $\bar{h}_{wet}$ for each donor represented within a treatment were then again

averaged to obtain the final value $\hat{h}_{wet}$ used in the desorption time course analyses.

The RH correction and averaging procedures used to estimate $\bar{h}_{wet}$ represent our best effort to adjust data obtained over a substantial period of time by several different workers. The use of outdoor RH values to estimate ambient RH in the laboratory was not optimum, but it did reflect a seasonal variation of the ambient tissue masses, m_{amb}, that was otherwise hard to explain. Like the averaging of m_{amb} over donor, it increased the precision of the results. The outdoor RH values ranged from 56% in the winter to 89% in the summer. According to the GAB isotherm [28], the relative thicknesses, h, of a single tissue sample maintained at these two RH values would be 1.00 and 1.29, respectively. Since diffusion time constants vary as h^2, the impact of this difference on calculated diffusvities is $(1.29)^2$ or a multiplicative factor of 1.66. By correcting for ambient RH as described, we estimate that the error introduced due to ambient RH differences was reduced from 66% to less than 30%. The latter value is comparable to typical within- or between-donor variabilities for excised human skin studies employing lipophilic permeants, and less than those for hydrophilic permeants [33].

The partition coefficient for each solute between the HSC membrane and the uptake solution was calculated for each individual sample as

$$K_{mv} = \frac{M^{\infty}}{\bar{h}_{wet} C_v} \qquad (5)$$

where C_v is the equilibrium concentration of solute in the uptake solution. A mean value of K_{mv} was then calculated for each treatment by averaging across donors.

2.5. Desorption time course analysis

A typical desorption curve for a hydrophilic compound is shown in Figure 1. The desorption

curves generally displayed an initial burst (the fast phase) followed by a period of much slower release (the slow phase) with associated amounts M_1^∞ and M_2^∞, respectively; thus $M^\infty = M_1^\infty + M_2^\infty$ The fractional amounts associated with these phases were consequently

$$f_1 = \frac{M_1^\infty}{M^\infty}; \qquad f_2 = \frac{M_2^\infty}{M^\infty} = 1 - f_1 \tag{6}$$

and the total amount desorbed at time t could be calculated as

$$M^t = M_1^t + M_2^t \tag{7}$$

Rearrangement of Eqs. (6) and (7) yields

$$\frac{M^t}{M^\infty} = f_1\left(\frac{M_1^t}{M_1^\infty}\right) + f_2\left(\frac{M_2^t}{M_2^\infty}\right) \tag{8}$$

Total fraction desorbed = rapid phase fraction + slow phase fraction

which was the central equation used to analyze the time course data.

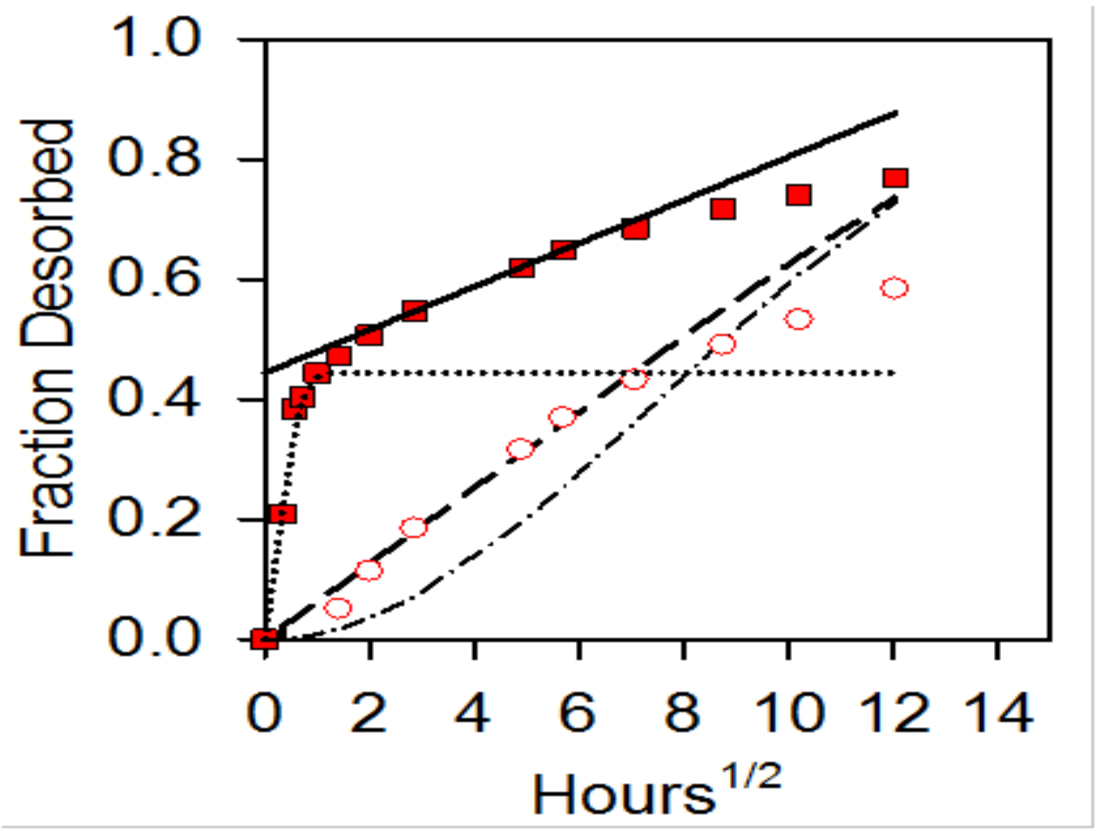

Fig. 1. Desorption of $^{22}Na^{+}$ from human SC equilibrated in 150 mM NaCl solution. The solid squares represent the mean of three skin donors, with one replicate per donor. The solid line shows a graphical method for estimating the fast phase fraction f_1; in this example $f_1 \approx 0.43$. Thus the dotted line represents the fast desorption phase $f_1 M_1^t/M_1^\infty$. The red circles represent fractional slow phase desorption M_2^t/M_2^∞ calculated after subtracting M_1^∞ from the original data. The dashed line represents Eq. (12) (Model 1) and the dash-dot line represents Eq. (14) (Model 3).

The rapid phase release, M_1^t, was assumed to be described by a homogeneous membrane solution of the form [34]

$$\frac{M_1^t}{M_1^\infty} = 1 - \frac{8}{\pi^2}\sum_{n=0}^{\infty}\frac{1}{(2n+1)^2}\exp\left(-\frac{(2n+1)^2\pi^2 D_1 t}{h_{wet}{}^2}\right) \qquad (9)$$

where D_1 is the effective diffusion coefficient for this process and h is the *total* thickness of the membrane (not the half thickness as in [34]). Equation (9) has the early time limit

$$\frac{M_1^t}{M_1^\infty} = 4\sqrt{\frac{D_1 t}{\pi h_{wet}{}^2}} \qquad (10)$$

Whether or not this treatment of the rapid phase desorption process is mechanistically correct, it yields a consistent method to deconvolve this relatively uninteresting feature of the desorption data from the much more interesting slow phase. In practice we found it was possible to obtain good initial estimates of M_1^∞ and D_1 by first estimating f_1 and M_1^∞ graphically as in Fig. 1, then estimating D_1 from the amount of solute released at the first sampling time, $M_1^{t_1}$; thus

$$D_1 = \frac{\pi {h_{wet}}^2}{t_1}\left(\frac{M_1^{t_1}/M_1^\infty}{4}\right)^2 \qquad (11)$$

The slow phase release was analyzed by three methods. Model I assumed only transverse diffusion throughout the membrane. In this respect it was entirely analogous to the rapid phase analysis; thus

$$\frac{M_2^t}{M_2^\infty} = 1 - \frac{8}{\pi^2}\sum_{n=0}^{\infty}\frac{1}{(2n+1)^2}\exp\left(-\frac{(2n+1)^2\pi^2 D_2 t}{{h_{wet}}^2}\right) \text{ Model I} \qquad (12)$$

An alternative model of the slow phase desorption in which material desorbs partly by transverse diffusion and partly by loss through skin appendages was also considered. Details are given in the Appendix. This model leads to the following expression:

$$\frac{M_2^t}{M_2^\infty} = 1 - \frac{8}{\pi^2}\exp(-kt)\sum_{n=0}^{\infty}\frac{1}{(2n+1)^2}\exp\left(-\frac{(2n+1)^2\pi^2 D_2 t}{{h_{wet}}^2}\right). \text{ Model II} \qquad (13)$$

In Model II, k is a first-order rate constant describing the exchange rate of permeant between the bulk HSC matrix and the skin appendages [19]. The exchange is considered to be accomplished via transient micropores in the epithelial cell membranes lining the appendages as described by Chizmadzhev et al. [4]; thus its value may, in principle, be size-dependent. The value of k for each test compound was determined by fits to the experimental desorption data, as described later. In the

limit $D_2 \rightarrow 0$, i.e. for permeants having negligible transverse permeation rates across the bulk HSC matrix, Eq. (13) has the simple limit,

$$\frac{M_2^t}{M_2^\infty} = 1 - \exp(-kt)\,.\,\text{Model III} \qquad (14)$$

In this limit there is no difference between the transverse concentration gradient in the membrane and that in the appendage; all permeant in the membrane diffuses laterally until it encounters a skin appendage, at which point it is transferred into the appendage through a network of micropores [4] and then cleared from the membrane by rapid diffusion in the appendage. We recognize that this approximation is somewhat unsatisfactory. A more careful analysis involving a large, but finite ratio of lateral to transverse diffusivities is possible (Fang Yu, unpublished data). The high ratio can be rationalized by considering the number of lipid bilayers that must be crossed for lateral versus transverse transport in the SC [35], and it is supported by recent experiments [35, 36].

The calculation was implemented by first graphically estimating f_1 and M_1^∞, then estimating D_1 from Eq. (11). Starting values for D_2 or k were subsequently obtained graphically (dashed line in Fig. 1), and the key parameters f_1 and D_2 (Model I) or f_1 and k (Model III) were further optimized using the Solver® add-in within Microsoft Excel® to obtain a least-squares solution. Example curve fits are shown in the Supplementary Material (Fig. S1). We found that Model I always led to better fits to the data than did Model III. Consequently, Model II calculations, which would fall in between Models I and III, were not performed.

Example curve fits are shown in the Supplementary Material (Fig. S1).

2.6 Cylindrical pore model calculations

Fits of the slow-phase diffusivity data to a cylindrical pore model were conducted as described

in Baswan et al. [37]. The model selected was the Renkin model [38], modified for solutes with $\lambda > 0.4$ as described by Deen [39]. This is a centerline approximation that does not consider electrostatic interactions or pore wall roughness; hence it must be considered as only a first estimate of the size-selectivity of the tissue. Details of the fitting procedure are given in the Supplementary Material.

2.7 Statistical analysis

Pairwise comparisons were conducted using the Student's *t*-test (two-tailed), with a significance level of $p < 0.05$. Multiple comparisons were made by two-way ANOVA, blocking by donor and treatment, with a significance level of $p < 0.10$. Fits to cylindrical pore models were evaluated using an *F*-test on the sum of squares residuals to determine the bounds on pore size [40]. Statistical tests were conducted using SigmaPlot® Vers. 12.5.

3. Results

3.1. Solute physicochemical properties

Relevant properties for the chemical compounds discussed in this study are shown in Table 1.

3.2. HSC membrane thickness and membrane/vehicle partition coefficient

Average HSC thicknesses and membrane/vehicle partition coefficients calculated according to Eqs. (1)-(5) are shown in Table 2. A more conservative estimate of $K_{sc/w}$ can be made by

Table 1 Physicochemical properties of the test solutes. The compounds are listed in order of increasing lipophilicity.

Chemical species	FW	log $K_{o/w}$ [a]	r_{se} [b] Å	D_{aq} [c] × 10^5 cm^2/s
$^{22}Na^+$	22.0	-	1.84	1.59
$^{36}Cl^-$	36.0	-	1.21	2.42
sucrose	342.3	–3.70	4.45	0.66
D-mannitol	182.2	–3.10	3.29	0.89

TEA^+	130.2	–2.82[d]	2.82	1.04
glycerin	92.1	–1.76	2.27	1.29
water	18.01	–1.38	1.10	2.73
niacinamide	122.1	–0.37	2.64	1.11
1-propanol	60.1	0.25	2.07	1.42
testosterone	288.4	3.32	4.87	0.60

[a] Measured values from Ref. [41].
[b] Hydrodynamic radius, calculated as described in the text.
[c] Aqueous diffusivity at 32°C calculated from Stokes-Einstein relationship using r_{se} value in Col. 4.
[d] Value cited is for the bromide salt.

Table 2 HSC thickness, uptake solution concentration, and mean membrane/vehicle partition coefficients (± donor SE) derived from the uptake/desorption studies. The quantity $f_2 = 1 - f_1$ is the slow phase fraction estimated from the desorption time course analysis (Col. 3 of Table 3).

Chemical species	$\hat{h}_{wet}$, μm	C_v, mM	K_{mv} (n_d,n_s)[a]	f_2K_{mv}	Reference
Na^+	39.0	0.15-150	2.37 ± 0.03 (3,12)[b]	1.74 ± 0.02	This study
Cl^-	74.3	0.15-150	0.95 ± 0.20 (3,12)[b]	0.45 ± 0.09	This study
sucrose	[43.4][c]	0.031	0.59 (1,1)	0.09	[17]
D-mannitol	55.7	0.15-150	0.85 ± 0.10 (3,12)[b]	0.39 ± 0.05	This study
TEA^+	36.5	0.15-150	1.40 ± 0.42 (3,12)[b]	0.48 ± 0.14	This study
glycerin	64.9	tracer	0.46 ± 0.06 (3,9)	0.31 ± 0.04	[16]
water	64.9	55.5	0.73 ± 0.04 (3,9)	0.50 ± 0.03	[16]
niacinamide	62.1	0.083	1.20 ± 0.10 (5,10-15)	0.87 ± 0.03	[15]
1-propanol	[43.4][c]	-[d]	1.1[d,e]	0.81[d,e]	[13]
testosterone	62.1	0.017	6.75 ± 0.61 (2,4-6)	6.75	[15]

[a] n_d and n_s are the number of donors and total number of samples, respectively.
[b] Partition coefficients are means of four concentration values. Some of these values were concentration dependent (cf. Fig. 2a).
[c] A priori value for thickness from Ref. [29].
[d] Limited details available in Ref. [13].
[e] Values cited are from Scheuplein and Blank [42] (n = 21, C_v = 100 mM).

assuming only the slowly desorbing fraction, $f_2 = 1 - f_1$, had been fully absorbed into the interior of the tissue. These values are tabulated in Col. 5 of Table 2. By either measure, all solutes except for sucrose had substantial occupancy of the membrane interior. Given the hydrophilicity of the first eight solutes (Na^+ - niacinamide), it is reasonable to expect that these compounds were largely distributed into aqueous regions of the tissue.

Results of the concentration studies with the three charged solutes and D-mannitol are shown in Fig. 2. K_{mv} values for Na^+ and TEA^+ showed significant changes with concentration (Fig. 2a).

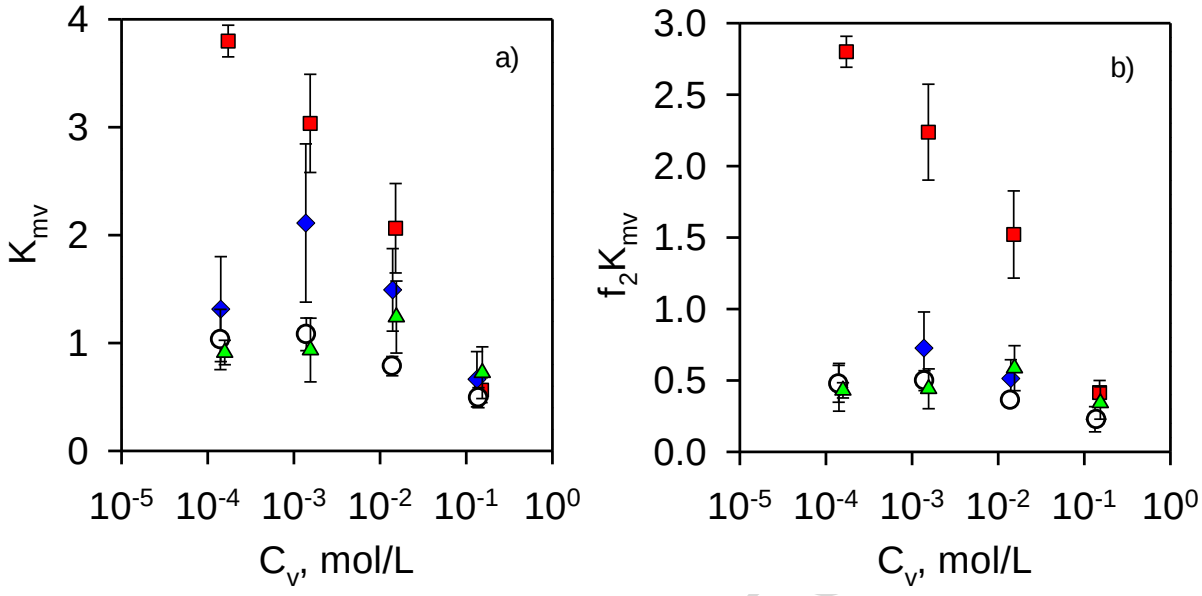

Fig. 2. HSC membrane/vehicle partition coefficients for Na^+ (squares), Cl^- (triangles), TEA^+ (diamonds) and mannitol (open circles) plotted as a function of concentration of the uptake solution, C_v. (a) Total partitioning, calculated as in Col. 4 of Table 2; (b) Slow phase fraction, calculated as in Col. 5 of Table 2. The values plotted are the mean ± SE of results from three skin donors, with one replicate per donor.

Values for all solutes were equivalent at the highest concentration tested (150 mM), but departed significantly at lower concentrations, where the values for Na^+ were several-fold higher than those for Cl^- and mannitol. The pattern for Na^+ and Cl^- is consistent with the Donnan effect in a negatively charged membrane, i.e. cations partition favorably into the membrane and anions are partially excluded. The differences are anticipated to diminish with increasing ionic strength and the resulting screening of the electrostatic potential [43]. TEA^+ showed a similar pattern to Na^+, except at the lowest concentration tested, 0.15 mM. This difference is possibly attributable to pH variations in the (unbuffered) test solutions – the pH rose with decreasing concentration in the NaCl solutions (to a value of 8.2 in the 0.15 mM solution), whereas it fell slightly with decreasing concentration in the TEAB solutions (to a value of 5.9 in the 0.15 mM solution). Thus the HSC membranes exposed to 0.15 mM TEAB may have had less fixed charge than those exposed to 0.15 mM NaCl. Partition coefficients calculated with respect to slowly desorbing material only (Fig.2b)

were not significantly different at any concentration for TEA^+, Cl^- and mannitol.

3.3. Desorption time course analysis

Representative time courses of desorption from isolated human SC for the solutes in Table 1 are shown in Fig. 3. Tabulated values for the full uptake/desorption dataset are included in the Supplementary Material. The desorption profiles for testosterone and 1-propanol (Fig. 3d), the most lipophilic compounds in this dataset, very closely matched that expected for a compound uniformly distributed in a homogeneous membrane, Eqs. (9) and (10). There was a linear region in the plot of fraction desorbed versus the square root of time (Eq. (10)), followed by a rapid attainment of a desorption plateau (Eq. (9)). This was not the case for the hydrophilic compounds. In most cases, there were two more-or-less linear portions of the desorption curves. The initial slopes, as determined from the first one or two desorption samples, were very steep. This phase was followed by a much more gradual release that persisted over a few hours (water) to more than six days (glycerin, niacinamide). The largest hydrophilic compound in the dataset, sucrose, showed a rapid release phase but very little slow phase desorption (Fig. 3b). Based on these observations, it is evident that only small amounts of sucrose partitioned into the interior of the tissue during the uptake phase of the experiment. For this reason, combined with the fact that there was only one observation, quantitative analysis of D_2 and k values was not attempted for sucrose.

The desorption curves were analyzed as described in Sect. 2.5 (cf. Fig. 1 and also Fig. S1 in the Supplementary Material). Summary parameters resulting from this analysis are listed in Table 3.

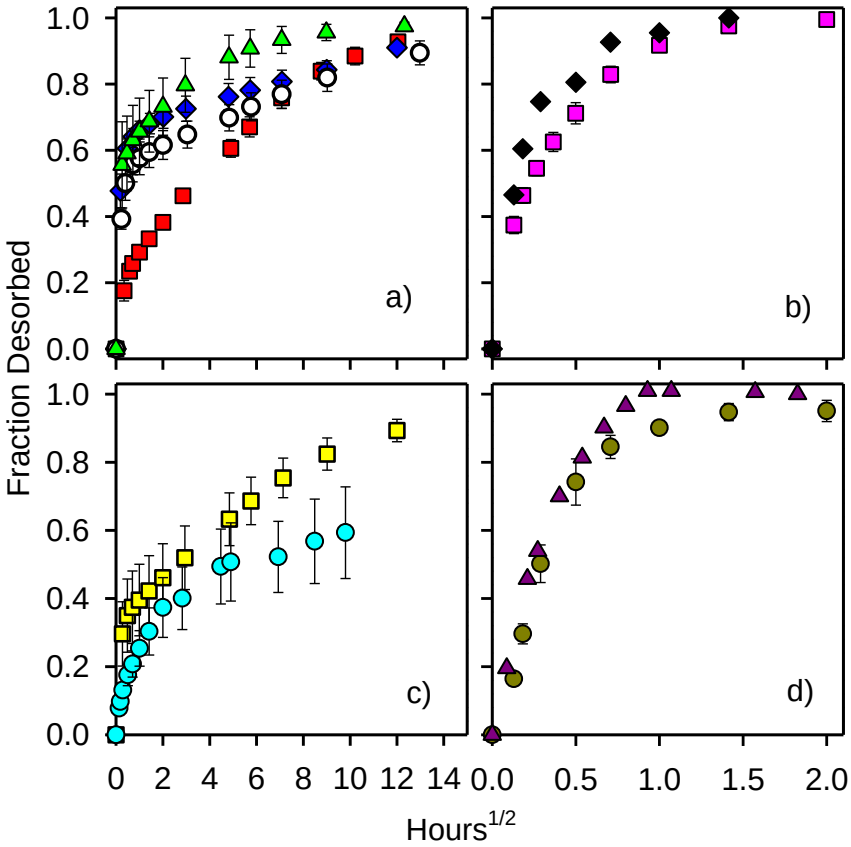

Fig. 3. Desorption time course of test compounds from HSC. (a) Na^+ (squares), Cl^- (triangles), TEA^+ (diamonds) and mannitol (circles) are from this study; (b) water [16] (squares) and sucrose [17] (diamonds); (c) niacinamide [15] (circles) and glycerin [16] (squares); (d) testosterone [15] (circles) and 1-propanol [13] (triangles). The values plotted are the mean ± SE of data from 1-5 donors, as shown in Table 2.

Table 3 Summary parameters arising from two-phase HSC desorption analysis

		Model I (Eq. 12)			Model III (Eq. 14)		
Chemical species	$D_1 \times 10^8$ cm^2/s	f_1	$D_2 \times 10^{11}$ cm^2/s	MSE	f_1	$k \times 10^6$ s^{-1}	MSE
Na^+	25	0.26	0.75	1.56	0.32	5.78	3.20
Cl^-	110	0.53	8.69	0.71	0.57	18.94	1.39
sucrose	1.33	0.81	-[a]	-	0.84	-[a]	-
D-mannitol	1.25	0.54	0.58	0.40	0.57	2.44	0.87
TEA^+	1.2	0.66	0.31	0.51	0.68	2.91	1.02
glycerin	70	0.33	1.78	0.50	0.38	5.18	1.63
water	1000	0.32	292	0.57	0.41	770	1.02
niacinamide	10	0.21	0.8	1.54	0.28	2.73	3.17
1-propanol	2.0	0.26	223	0.20	0.42	1131	0.24
testosterone	-	0	350		-	-	-

[a] Not calculated due to insufficient slow-phase data.

When analyzed in terms of the physicochemical properties in Table 1, several significant relationships were found, as discussed in the following paragraphs.

3.3.1 Fast phase desorption

Fig. 4 shows a plot of the fast phase desorption fraction, f_1, as a function octanol/water partition coefficient for the solutes in Table 3 with reported values of $K_{o/w}$. There was a strong inverse relationship between these variables (r^2 = 0.927). However, there was also a moderate positive correlation (r^2 = 0.40) between f_1 and hydrodynamic radius, r_{se}, for these solutes. Thus, it may be stated that large, hydrophilic solutes had higher fast phase desorption fractions. Fast phase diffusivities, D_1, were not related to the properties in Table 1 in any obvious manner. The most notable value was that of water, 1.0×10^{-5} cm^2s^{-1}, which is about 1/3 of its aqueous diffusivity value of 2.73×10^{-5} cm^2s^{-1} at 32°C (Table 1).

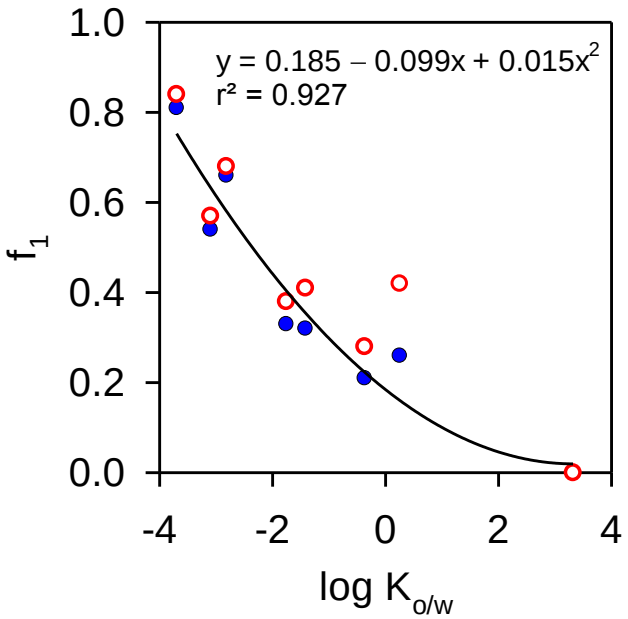

Fig. 4. Fast-phase desorption fraction as a function of hydrophilicity for the solutes in Table 3 with reported values of $K_{o/w}$. Closed circles – Model I; open circles – Model III. The trendline is fit to the Model I data.

3.3.2. Slow phase desorption

Slow phase diffusivity values, D_2, and also those of the appendageal exchange constant, k, were found to be strong functions of molecular size as represented by r_{se}. The relationships held for both charged and uncharged solutes, with the exception of water, propanol and testosterone, which had values of D_2 and k at least 30-fold higher than would be expected from the trend. Plots are shown in Fig. 5. The values for the other six solutes were well represented by power laws, i.e.

$$D_2 = 9.98 \times 10^{-11}\, r_{se}^{-2.76}\ \text{cm2s–1}\, r2 = 0.73\ \text{(Model I)} \quad (15)$$

$$k = 25.2 \times 10^{-6}\, r_{se}^{-2.09}\ \text{s–1}\, r2 = 0.96\ \text{(Model III)} \quad (16)$$

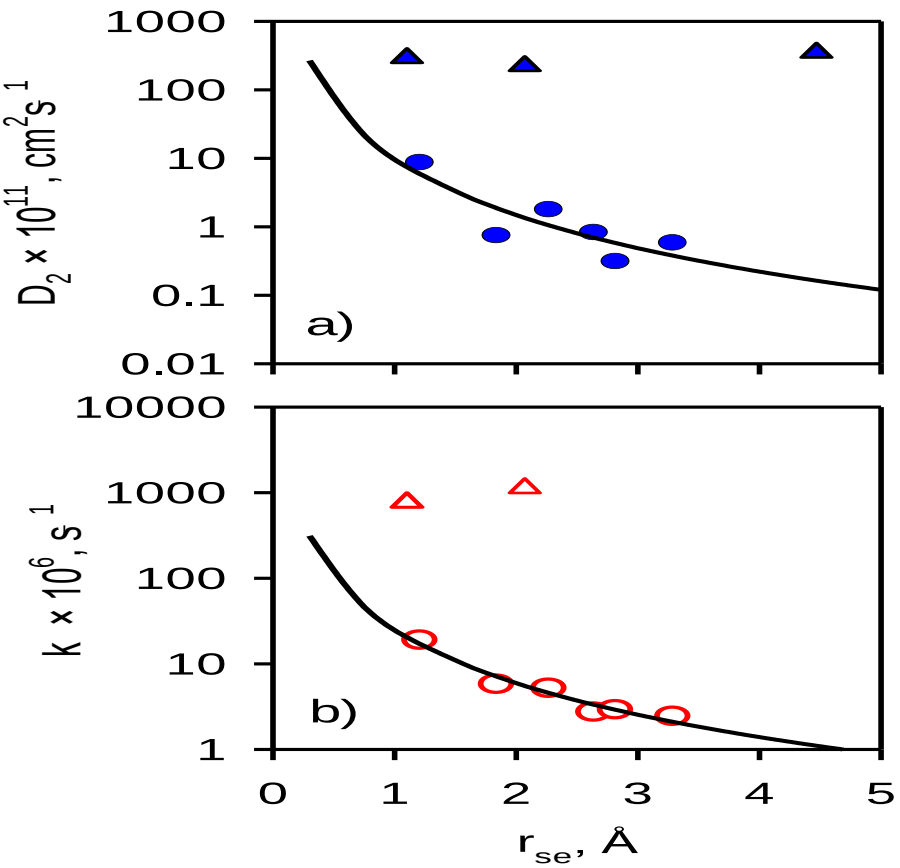

Fig. 5. Slow phase transport parameters for SC desorption analysis. The data are taken from Tables 1 and 3. (a) Model I;(b) Model III. The smooth curves represent Eqs. (15) and (16). The outlying values (triangles) are those for water, 1-propanol, and testosterone, permeants that diffuse readily through the stratum corneum lipid/corneocyte composite matrix [29, 44].

Model I analysis and the Model III analysis were similar. Model II yielded results intermediate between Model I and Model III. The fits of Model I to the desorption time course data were in all cases superior to fits of Models II or III, as judged by significantly lower values of the mean squared error (MSE) values in Table 3. However, it is evident from Eqs. (15) and (16) that the size dependencies derived from both the Model I analysis and the Model III analysis were similar. Model II yielded results intermediate between Model I and Model III.

4. Discussion

Desorption measurements represent a complementary method to permeability measurements to determine membrane transport properties of exogenous solutes. They are less sensitive to membrane imperfections [15], but more sensitive to asymmetry in membrane structure and properties [15, 45, 46]. They readily yield membrane/vehicle partition coefficients, and they yield time constants related to the quantity h^2/D. In our experience with HSC, these time constants are more consistent than those obtained from permeability time lags, usually interpreted as $h^2/6D$. Highly and moderately lipophilic compounds, e.g. testosterone [15] and propanol [13] evidently yield SC desorption profiles largely consistent with homogeneous membrane behavior, but the eight hydrophilic compounds discussed in this report do not. Each requires at least two time constants in order to describe the desorption time course. For six of the eight hydrophilic solutes (Na^+, Cl^-, TEA^+, mannitol, glycerin and niacinamide) the slow desorption phase was very prolonged, with time courses extending 144 h or longer (Fig. 2, Panels a and c) and associated diffusion constants, D_2, with values less than 2×10^{-11} cm^2/s (Table 3, Col. 4). Time constants (τ_d) for these curves estimated as $\hat{h}_{wet}{}^2/D_2$ (with $\hat{h}_{wet}$ taken from Table 2) ranged from 176 h for Cl^- to 1340 h for niacinamide. The slow desorption process was thus much more prolonged than the slowly reversible keratin binding phenomena reported elsewhere [20-23]. For example, τ_d values for

desorption from keratin reported by Seif and Hansen [22], calculated as $1/k_{off}$, range from 0.58 h for caffeine to 6.4 h for nortriptyline at pH 8. At pH 5.5, where nortriptyline was highly ionized, τ_d decreased to 1.6 h. Calculated in this manner, Anissimov and Roberts' study of water desorption from HSC leads to τ_d = 0.37 h, whereas Frasch et al.'s study of theophylline permeation through human epidermis leads to τ_d = 2.1 h. It is evident from the comparison that slowly reversible binding is not likely to be the rate-limiting process for these six hydrophilic permeants. In fact, it is difficult to invoke binding to explain this behavior for two additional reasons: (1) Equilibrium binding to keratinaceous substrates correlates directly with lipophilicity, with hydrophilic solutes binding weakly or not at all [47]; and (2) A binding mechanism does not explain how these lipid membrane-impermeable solutes reached either the cornified cell envelope or the corneocyte interior in the first place. There must be a transport pathway for hydrophilic solutes connecting the corneocytes. Be it lipid defects or transport within the desmosomes, this is the likely source of slow desorption rates.

These measurements and the associated analysis provide additional evidence for a size-selective polar pathway in HSC that allows access into corneocyte interiors for small, hydrophilic solutes. The second part of this statement simply recognizes that most of the water in hydrated HSC resides in corneocytes. Based on our measurements, small, hydrophilic solutes in the membrane, when at equilibrium with external solutions, occupy a substantial fraction of this water. But what is the evidence for size-selectivity beyond the $1/r_{se}$ behavior characteristic of aqueous diffusion? Part of the answer lies in the extensive body of literature regarding skin permeability to hydrophilic solutes [5], skin electrical properties [37, 48], transdermal iontophoresis [49] and sonophoresis [6]. These sources support the existence of aqueous pathways through the stratum corneum with pore radii ranging from 16 Å [37] to 32 Å [6]. The data in Table 3 and Fig. 5 provide

additional evidence for such pathways. To show this, we divided the D_2 and k values in Table 3 by the D_{aq} values at 32°C in Table 1 and plotted the results versus r_{se}. Such a plot tests for evidence of hindered diffusion [37]. The results are shown in Fig. 6. The residual size dependency shown in this plot further confirms that the transport pathway is size-selective. We compared these plots with the predictions of a cylindrical pore model as described in [37]. The optimum pore radius based on Model I (Fig. 6a) was r_p = 8.5 Å and on Model III (Fig. 6b) was r_p = 11.3 Å. However, pores as large as 20 Å could be accommodated without significantly degrading either fit. Details of this analysis are presented in the Supplementary Material. We consider the result to be fully consistent

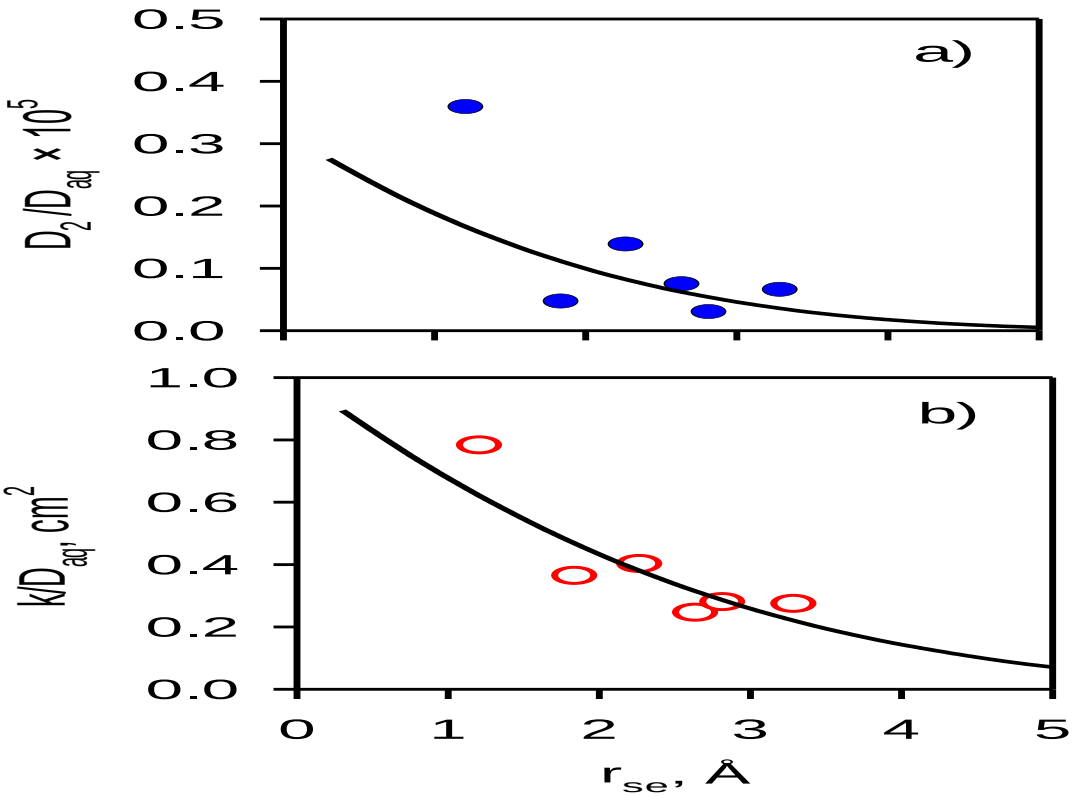

Fig. 6. Fits of slow phase desorption data from HSC (Cl^-, Na^+, TEA^+, D-mannitol, niacinamide and glycerin) to a cylindrical pore model. (a) Model I, r_p = 8.5 Å; (b) Model III, r_p = 11.3 Å.

with the value r_p = 16 Å for split-thickness human skin estimated by Baswan et al. [37] on the basis of electrical conductivity and transport number measurements and the value r_p = 20 Å estimated by Peck et al. [5] from steady-state permeability measurements on human epidermal membrane.

Desorption rates of water, 1-propanol, testosterone and sucrose from HSC were much faster than those of the other six permeants (Fig. 3) and were not included in the analysis leading to Eqs. (15) and (16). For sucrose it is evident from the limited data reported here that not much permeant reached the interior of the tissue, with rapidly desorbing material accounting for more than 80% of the total (Table 3). There is a real chance that equilibrium partitioning was not achieved during the uptake phase of the experiment. The other three compounds are known to be membrane-permeable due either to their small size (water), lipophilicity (testosterone) or a combination of these factors (1-propanol) [29, 44]. It is not surprising they did not match the pattern of the other six permeants. More surprising to us was the fact that results for the six hydrophilic permeants (excluding sucrose) were so closely related. Glycerol and niacinamide are small, uncharged hydrophilic permeants that have calculated steady-state skin permeability coefficients (P_{sc}) much higher than the other four permeants, according to two established lipid membrane models – see Columns 4 and 5 of Table 4.

Table 4 Steady-state skin permeabilities (P_{sc}) of the poorly-membrane permeable solutes, obtained by four different methods. Values are expressed in units of cm/h, multiplied by 10^5.

Chemical species	Permeation Database (n_s)[a]	Desorption Analysis[b]	Potts-Guy equation [50]	Wang et al. calculation [44]	Ref.[c]
Na^+	1.9 ± 0.4 (28)	1.20	-	-	[51]
Cl^-	-	1.89	-	-	
sucrose	2.1 ± 0.5 (10)[d]	-	0.0037	0.0008	[5]
D-mannitol	4.1 ± 0.1 (9)[d]	0.15	0.093	0.028	[5]
TEA^+	5.6(1), 8.8(1)[e]	0.15	0.30	0.16	[52]
glycerin	56 ± 15 (9)[f]	0.31	2.9	2.8	[16]
niacinamide	4.9 ± 0.8 (31)	0.40	19	17	[15]

[a] Steady state skin permeabilities (mean ± SE across donors) taken from the literature. n_s is the total number of skin samples represented.
[b] This study. Results are calculated as $f_2\, D_2\, K_{mv}/\hat{h}_{wet}$, using results from Tables 2 and 3.
[c] Reference for steady-state skin permeability values listed in Column 2.
[d] 37°C values
[e] 27 and 39°C values, respectively.
[f] By contrast, the permeability of glycerin through mouse skin is 14×10^{-5} cm/h [53].

Yet their skin permeabilities as inferred from the desorption studies (Column 3, Table 4) are much smaller than the model predictions. Skin permeabilities determined in steady-state permeation

experiments (Column 2, Table 4) were one to two orders of magnitude higher than those inferred from desorption studies for four of the six permeants. This pattern has been noted before [15, 16]. It is a reminder that experimental transport results on heterogeneous membranes like HSC depend exquisitely on the method used to make the measurement.The role of skin appendages, i.e. hair follicles and sweat ducts, in topical and transdermal absorption has been the subject of much research. Much of the discussion has concerned hair follicles and their associated sebaceous glands [54]. Percutaneous absorption of compounds as polar as caffeine (log K_{oct} = –0.07) has been shown to be substantially impacted by follicular transport [55]. Sweat ducts have largely been ignored in these discussions except in the iontophoresis literature, where they have been strongly implicated in the transport of ions into the skin [4, 56, 57]. They are clearly not transdermal delivery routes when the skin is actively sweating, as rapid sweat secretion would surely overwhelm outside-in diffusion. But this is not the normal state of the sweat gland when an individual is at rest. In excised human skin in vitro, sweat ducts have been considered by some to be swollen shut.

In the present study, which involves just one skin layer, the stratum corneum, it is not necessary to invoke appendageal transport to explain the results. A transcellular diffusion model involving hindered diffusion of highly hydrophilic species through lipid defects/desmosomes connecting the corneocytes (Model I) gives a better representation of the results than does a simplified appendageal transport model (Model III) or a combination of the two (Model II). This is not surprising since desorption rates are not very sensitive to membrane defects having small surface areas [15]. A skin appendage, or the remnants thereof in isolated HSC, may be thought of as a membrane defect. We include appendageal models in the analysis presented here because it is highly likely that skin appendages play a role in both transient and steady-state absorption of hydrophilic compounds [4, 56, 57].

Finally, it is of interest to consider the role of tortuosity in the transport of polar compounds

through the SC. Tortuosity played a significant role in Mitragotri's SC porous pathway network [10], counteracting the effect of hindered diffusion by allowing large solutes a more direct path across the SC than small solutes [58]. In fact, the size-selectivity characteristics of the Mitragotri model for polar solutes do not differ greatly from that of water alone due to this cancellation (J. Jaworska, personal communication). The physical models presented here do not require a tortuosity factor, and the reported size-selectivity couched in terms of small, cylindrical pores arises naturally from the analysis (cf. Fig. 6). We assign no particular credence to the estimated pore radius of 8-12 Å due to the uncertainties in both the measurement and the simplified hindered diffusion analysis. However, the desorption data presented here provide strong evidence that highly hydrophilic solutes with low lipid membrane permeabilities leak into and out of SC corneocytes by a size-selective mechanism.

5. **Conclusions**

Uptake/desorption measurements on hydrophilic compounds in isolated human stratum corneum confirm that substantial amounts of these compounds absorb into the interior of the and desorb very slowly. The desorption rates were consistent with hindered diffusion through cylindrical aqueous pores having an optimum radius of 8-12 Å. The slow phase desorption process could be described in terms of a transverse transport model or an appendageal exchange model. The former was more effective in matching the desorption profiles.

Acknowledgements

This work was supported by a grant from the Cefic Long Range Initiatives program (LRI-B13) and by National Science Foundation GOALI Award #1335822. The opinions presented are those of the authors and have not been endorsed by the sponsors. The authors report no conflict of interest.

Appendix: Two pathway model for slow desorption of hydrophilic compounds from human stratum corneum (Model II in main text)

The analysis presented here describes only the slow phase of desorption of solutes from the SC as discussed in the text (cf. Eqs. 6-8 and Fig. 1). It is conceived within the context of an appendageal model for hydrophilic solute transport through skin under development in our laboratories [18, 19]. The general idea is shown in Fig. A1. Solute is considered to be initially distributed homogeneously within a thin membrane (the stratum corneum) punctuated by cylindrical shunts (skin appendages including sweat ducts and sebaceous ducts). The "homogeneous distribution" is actually a homogenized approximation to the brick-and-mortar microscopic transport model of Wang et al. [29, 44], most recently summarized in Dancik et al. [59]. Thus, the underlying microscopic structure involves a two-dimensional array of corneocytes surrounded by anisotropic bilayer lipids. Hydrophilic solutes are presumed to reside primarily within the corneocyte phase, and to slowly leak through the lipid layers separating the corneocytes by means of lipid defects or (possibly) desmosomes. Due to the high aspect ratio of the corneocytes, lateral diffusion in this model is inherently more rapid than transverse diffusion, as more fewer lipid bilayers must be crossed in order to traverse comparable distances. This statement is supported by the fact that lateral diffusion coefficients in the upper SC have been found to be between 170 and 2100 times larger than transverse diffusion coefficients, both in our laboratory [35] and in others [36], as discussed by Rush et al. [35]. At time $t = 0$, the membrane is placed in contact with a large volume of well-stirred aqueous solution, and any solute adhered to the membrane or distributed within the shunts rapidly desorbs. This process is represented by Eq. (9) in the main text. For the Model II approximation, the rapidly desorbed material is considered to be completely removed from

the system at time zero; thus the concentration of the solute external to the membrane *and* within the shunts is taken to be zero.

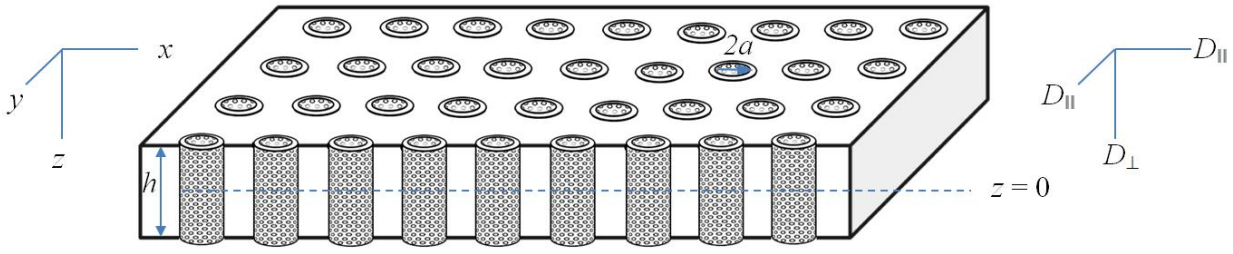

Fig. A1. Conceptual model for desorption from a membrane of thickness h punctuated by a regular array of cylindrical shunts of radius a. Solute diffusivity is taken to be isotropic in the plane of the membrane ($D_{\parallel}$), but to have a different value in the transverse direction ($D_{\perp}$). Solute is cleared either at the transverse boundaries of the membrane ($z = \pm h/2$) or by a hindered diffusion process at the perimeter of the shunts as described in the text.

Solute transport within the continuous region of the membrane (not including the shunts) is governed by the diffusion equation,

$$\frac{\partial c}{\partial t} = \vec{D}\nabla^2 c = D_{\parallel}\left(\frac{\partial^2 c}{\partial x^2} + \frac{\partial^2 c}{\partial y^2}\right) + D_{\perp}\frac{\partial^2 c}{\partial z^2} \qquad \text{(A1)}$$

where $D_{\parallel}$ and $D_{\perp}$ represent lateral and transverse diffusivities, respectively, and $c = c(x,y,z)$ has gradients in all spatial dimensions. The boundary conditions include $c = 0$ at $z = \pm h/2$ and a hindered diffusion process at the perimeter of the shunts that can be qualitatively expressed as

$$D_{\parallel}\frac{\partial c}{\partial r}\Big|_{r=a} = P_{duct}\, c\Big|_{r=a} \qquad \text{(A2)}$$

where r is a radial coordinate with its origin at the center of a pore, P_{duct} is the permeability of the epithelial cell membrane(s) lining the shunt [19], and the expression is to be evaluated at the perimeter of each pore. As described in the main text, the value of P_{duct} is expected to be dependent

on the size of the diffusing permeant, as P_{duct} represents the proportionality constant for diffusive transport through transient micropores in the epithelial cell membranes lining the appendage.

To solve the boundary value problem suggested by Eqs. A1 and A2 precisely, one must specify the arrangement of the cylindrical shunts, define a unit cell about a single shunt, and solve Eqs. 1 and 2 within this cell with periodic boundary conditions in the *xy* plane. The general solution to this problem is sensitive to the detailed geometry of the shunt array and can be obtained numerically (Fang Yu, unpublished data), but it is not our intention to do this here. Instead, a simpler model will be investigated. We consider the limit of the model as $a \rightarrow 0$ and the shunt density N increases as $1/a$, so that the total shunt surface area within the membrane (which is proportional to $2\pi aN$) remains constant. In such a limit, lateral diffusion is not rate-limiting. This is a distributed clearance model similar to the approach we have used for dermis [60]. Under these conditions, the conceptual model can be represented by the following partial differential equation:

$$\frac{\partial c}{\partial t} = D_{\perp}\frac{\partial^2 c}{\partial z^2} - kc \quad \left(-\frac{h}{2} \leq z \leq \frac{h}{2}\right). \quad \text{(A3)}$$

The first term on right side describes permeant desorption from the sides of the tissue (transverse diffusion) and the second term describes the loss through the shunts. In the limit cited, the clearance constant k in Eq. A3 is numerically equivalent to $2\pi aNP_{duct}$ in Eq. A2. The value of k is insensitive to the geometry of the appendageal array; it is equal to the ratio of the total surface area of the shunts $2\pi aNh$ within a volume of tissue having unit area and thickness h. This volume contains N shunts. The concentration within the membrane, $c = c(z,t)$, is now a function of one spatial dimension only, i.e. it is homogeneous within the *xy*-plane.

Due to symmetry, Eq. (A3) is solved over half the membrane, $0 \leq z \leq h/2$. The initial condition (IC) and boundary conditions (BCs) governing the problem are, respectively,

$$c(z,0) = \mathrm{c}_2^0 \quad \text{(A4)}$$

$$\begin{cases} \left.\frac{\partial c}{\partial z}\right|_{z=0} = 0 \\ c\left(\frac{h}{2}, t\right) = 0. \end{cases} \quad \text{(A5)}$$

where c_2^0 is the concentration of material remaining after the rapid desorption phase is complete. The integral of $c(z,0)$ across the membrane is equal to initial amount of solute per unit area or, equivalently, to the total amount that will desorb at infinite time, M_2^∞, if there is no binding or degradation, i.e.

$$M_2^\infty = 2c_0 \int_0^{\frac{h}{2}} dz = \mathrm{c}_2^0 h \quad \text{(A6)}$$

Dividing each variable by a characteristic value, one can transform Eq. (A3) into the dimensionless form

$$\frac{\partial \hat{c}}{\partial \tau} = \frac{\partial^2 \hat{c}}{\partial \hat{z}^2} - \alpha \hat{c} \quad \text{(A7)}$$

where $\hat{c} = \frac{c}{\mathrm{c}_2^0}, \hat{z} = \frac{2z}{h}, \ \tau = \frac{4D_\perp t}{h^2}$ and $\alpha = \frac{k h^2}{4D_\perp}$.

The corresponding IC and BCs are:

$$\hat{c}(\hat{z},0) = 1 \quad \text{(A8)}$$

$$\begin{cases} \left.\frac{\partial \hat{c}}{\partial \hat{z}}\right|_{\hat{z}=0} = 0 \\ \hat{c}(1,\tau) = 0 \end{cases} \quad \text{(A9)}$$

Eq. (A7) was solved by separation into two ordinary differential equations (ODEs), i.e.

$\hat{c}(\hat{z},\tau) = g(\tau)f(\hat{z})$ (A10)

After setting $\frac{g'}{g} + \alpha = \frac{f''}{f} = -\lambda^2$, the two ODEs can be represented as Eqs (A11) and (A12), respectively.

$g' = (-\alpha - \lambda^2)g$ with $g(0) = 1$ (A11)

$f'' = -\lambda^2 f$ with $f(1) = 0$ (A12)

The analytical solutions to these equations are

$g = e^{(-\alpha-\lambda^2)\tau}$ (A13)

$f = \sum_{n=0}^{\infty} d_n \cos(\lambda\hat{z})$ (A14)

where $d_n = \frac{4\cos(n\pi)}{(2n+1)\pi} = \frac{4(-1)^n}{(2n+1)\pi}$. The quantities $\lambda = \frac{2n+1}{2}$ and $\cos(\lambda\hat{z})$ are eigenvalues and eigenfunctions, respectively.

The concentration profile can be therefore be written in dimensionless form as

$$\hat{c}(\hat{z},\tau) = \frac{4}{\pi}\sum_{n=0}^{\infty}\frac{(-1)^n}{2n+1}e^{\left[-\alpha-\left(\frac{2n+1}{2}\right)^2\pi^2\right]\tau}\cos\left(\frac{2n+1}{2}\right)\pi\hat{z} \quad 0 \le \hat{z} \le 1 \qquad \text{(A15)}$$

Restoring the dimensional variables and also the lower half of the membrane yields

$$c(z,t) = \frac{4c_2^0}{\pi}\sum_{n=0}^{\infty}\frac{(-1)^n}{2n+1}e^{-\left[k+\frac{(2n+1)^2\pi^2 D_\perp}{h^2}\right]t}\cos\left(\frac{(2n+1)\pi z}{h}\right) \quad -\frac{h}{2} \le z \le \frac{h}{2} \quad \text{(A16)}$$

The integral of $c(z,t)$ within the membrane is equal to remaining dose (or total amount of permeant per unit area, M_2^{rt}, at time t as shown in Eq. (A17):

$$M_2^{rt} = \frac{8hc_2^0}{\pi^2} e^{-kt} \sum_{n=0}^{\infty} \frac{1}{(2n+1)^2} e^{-\left[\frac{(2n+1)^2\pi^2 D_\perp t}{h^2}\right]} \quad \text{(A17)}$$

Here we have also removed the term e^{-kt} from the summation because it does not depend on n. Recalling that $M_2^{\infty} = hc_2^0$, the amount of permeant desorbed at time t can therefore be formulated as:

$$M_2^t = M_2^{\infty}\left[1 - \frac{8}{\pi^2} e^{-kt} \sum_{n}^{\infty} \frac{1}{(2n+1)^2} e^{-\left(\frac{(2n+1)^2\pi^2 D_\perp t}{h^2}\right)}\right] \quad \text{(A18)}$$

Dividing Eq. (A18) by M_2^{∞}, with the identification $D_\perp = D_2$, yields Eq. (13) in the main text.

References

[1] J. Bouwstra, F.E.R. Dubbelaar, G.S. Gooris, M. Ponec, The lipid organisation in the skin barrier, Acta Derm. Venereol. 208 (2000) 23-30.

[2] R.T. Tregear, The permeability of mammalian skin to ions, J. Invest. Dermatol. 46 (1966) 16-23.

[3] G.B. Kasting, L.A. Bowman, DC electrical properties of frozen, excised human skin, Pharm. Res. 7 (1990) 134-143.

[4] Y.A. Chizmadzhev, A.V. Indenbom, P.I. Kuzmin, S.V. Galichenko, J.C. Weaver, R.O. Potts, Electrical properties of skin at moderate voltages: contribution of appendageal macropores, Biophys. J. 74 (1998) 843-856.

[5] K.D. Peck, A.-H. Ghanem, W.I. Higuchi, Hindered diffusion of polar molecules through and effective pore radii estimates of intact and ethanol treated human epidermal membranes, Pharm. Res. 11 (1994) 1306-1314.

[6] H. Tang, S. Mitragotri, D. Blankschtein, R.S. Langer, Theoretical description of transdermal transport of hydrophilic permeants: application to low-frequency sonophoresis, J. Pharm. Sci. 90 (2001) 545-568.

[7] H. Tang, D. Blankschtein, R.S. Langer, Prediction of steady-state skin permeabilities of polar and nonpolar permeants across excised pig skin based on measurements of transient diffusion: characterization of hydration effects on the skin porous pathway, J. Pharm. Sci. 91 (2002) 1891-1907.

[8] Y.N. Kalia, A. Naik, J. Garrison, R.H. Guy, Iontophoretic drug delivery, Adv. Drug Deliv. Revs. 56 (2004) 619-658.

[9] A. Azagury, L. Khoury, G. Enden, J. Kost, Ultrasound mediated transdermal drug delivery, Adv. Drug Deliv. Revs. 72 (2014) 127-143.

[10] S. Mitragotri, Modeling skin permeability to hydrophilic and hydrophobic solutes based on four permeation pathways, J. Control. Rel. 86 (2003) 69-92.

[11] R.O. Potts, M. Francoeur, The influence of stratum corneum morphology on water permeability, J. Invest. Dermatol. 96 (1991) 495-499.

[12] L. Chen, L. Han, G. Lian, Recent advances in predicting skin permeability of hydrophilic solutes, Adv. Drug Deliv. Rev. 65 (2013) 295–305.

[13] E.R. Cooper, B. Berner, Skin permeability, in: D. Skerrow, C.J. Skerrow (Eds.) Methods in Skin Research, John Wiley and Sons, New York, 1985, pp. 407-432.

[14] S. Mitragotri, In situ determination of partition and diffusion coefficients in the lipid bilayers of stratum corneum, Pharm. Res. 17 (2000) 1026-1029.

[15] G.B. Kasting, M.M. Miller, P.S. Talreja, Evaluation of stratum corneum heterogeneity, in: R.L. Bronaugh, H.I. Maibach (Eds.) Percutaneous Absorption, Taylor & Francis, New York, 2005, pp. 193-212.

[16] S.A. Ventura, G.B. Kasting, Dynamics of glycerin and water transport across human skin from binary mixtures, Int. J. Cosmet. Sci. online in advance of print, doi: 10.1111/ics.12362 (2016).

[17] P.S. Talreja, Determination of transport pathways in human stratum corneum: micro and macro measurements, M.S. thesis, College of Pharmacy, University of Cincinnati, Cincinnati, OH, 2000.

[18] G.B. Kasting, M.A. Miller, J. Jaworska, A new approach to modeling the skin's polar pathway, Interpore Society Annual Meeting, Cincinnati, OH, May, 2016.

[19] G.B. Kasting, M.A. Miller, An appendageal model for the transport of hydrophilic compounds across the skin, Occupational and Environmental Exposures to Skin, Manchester, UK, Sept., 2016.

[20] Y.G. Anissimov, M.S. Roberts, Diffusion modelling of percutaneous absorption kinetics: 4. Effects of a slow equilibration process within stratum corneum on absorption and desorption kinetics, J. Pharm. Sci. 98 (2009) 772-781.

[21] D.G. Petlin, M. Rybachuk, Y.G. Anissimov, Pathway distribution model for solute transport in stratum corneum, J. Pharm. Sci. 104 (2015) 4443–4447.

[22] S. Seif, S. Hansen, Measuring the stratum corneum reservoir: desorption kinetics from keratin, J. Pharm. Sci. 101 (2012) 3718-3728.

[23] H. Frasch, A. Barbero, J. Hettick, J. Nitsche, Tissue binding affects the kinetics of theophylline diffusion through the stratum corneum barrier layer of skin, J. Pharm. Sci. 100 (2011) 2989–2995.

[24] R.A. Robinson, R.H. Stokes, Electrolyte solutions, the measurement and interpretation of conductance, chemical potential, and diffusion in solutions of simple electrolytes, 2nd ed., Butterworths, London, 1970.

[25] H. Yasuda, C.E. Lamaze, A. Peterlin, Diffusive and hydraulic permeabilities of water in water-swollen polymer membranes, J. Polymer Sci. A-2, 9 (1971) 1117-1131.

[26] S. Baswan, S.K. Li, G.B. Kasting, Diffusion of uncharged solutes through human nail plate, Pharm. Devel. Technol. 21 (2016) 255-260.

[27] A.M. Kligman, E. Christophers, Preparation of isolated sheets of human stratum corneum, Arch. Dermatol. 88 (1963) 702-705.

[28] X. Li, R. Johnson, B. Weinstein, E. Wilder, E. Smith, G.B. Kasting, Dynamics of water transport and swelling in human stratum corneum, Chem. Eng. Sci. 138 (2015) 164-172.

[29] T.-F. Wang, G.B. Kasting, J.M. Nitsche, A multiphase microscopic model for stratum corneum permeability. I. Formulation, solution and illustrative results for representative compounds, J. Pharm. Sci. 95 (2006) 620-648.

[30] N.D. Barai, Effect of hydration on skin permeability, M.S. thesis, College of Pharmacy, University of Cincinnati, Cincinnati, OH, 2002.

[31] G.B. Kasting, N.D. Barai, Equilibrium water sorption in human stratum corneum, J. Pharm. Sci. 92 (2003) 1624-1631.

[32] I.H. Blank, J. Moloney, A.G. Emslie, I. Simon, C. Apt, The diffusion of water across the stratum corneum as a function of its water content, J. Invest. Dermatol. 82 (1984) 183-194.

[33] P. Liu, J.A.S. Nightingale, T. Kurihara-Bergstrom, Variation of human skin permeation in vitro: Ionic vs neutral compounds, Int. J. Pharm. 90 (1993) 171-176.

[34] J. Crank, The Mathematics of Diffusion, 2nd ed., Clarendon Press, Oxford, 1975.

[35] A.K. Rush, M.A. Miller, E.D. Smith, G.B. Kasting, A quantitative radioluminographic imaging method for evaluating lateral diffusion rates in skin, J. Control. Rel. 216 (2015) 1-8.

[36] Y.G. Anissimov, X. Zhao, M.S. Roberts, A.V. Zvyagin, Fluorescence recovery after photo-bleaching as a method to determine local diffusion coefficient in the stratum corneum, Int. J. Pharm. 435 (2012) 93-97.

[37] S. Baswan, S.K. Li, T.D. LaCount, G.B. Kasting, Size and charge dependence of ion transport in human nail plate, J. Pharm. Sci. 105 (2016) 1201–1208.

[38] J.R. Pappenheimer, E.M. Renkin, L.M. Borrero, Filtration, diffusion and molecular sieving through peripheral capillary membranes. A contribution to the pore theory of capillary permeability, Am. J. Physiol., Reg.Integ. Comp. Physiol. Vol. 15 167 (1951) 13-46.

[39] W. Deen, Analysis of Transport Phenomena, Oxford University Press, London, 1998.

[40] P.R. Bevington, Data Reduction and Error Analysis for the Physical Sciences, McGraw-Hill, New York, 1969.

[41] US_EPA, Estimation Programs Interface Suite™ for Microsoft® Windows, in, United States Environmental Protection Agency, Washington, DC, USA, 2009.

[42] R.J. Scheuplein, I.H. Blank, Mechanism of percutaneous absorption. IV. Penetration of nonelectrolytes (alcohols) from aqueous solutions and from pure liquids, J. Invest. Dermatol. 60 (1973) 286-296.

[43] P.F. Curran, S.G. Schultz, Transport across membranes: general principles, in: Handbook of Physiology, Waverly Press, Baltimore, MD, 1968, pp. 1217-1243.

[44] T.-F. Wang, G.B. Kasting, J.M. Nitsche, A multiphase microscopic model for stratum corneum permeability. II. Estimation of physicochemical parameters and application to a large permeability database, J. Pharm. Sci. 96 (2007) 3024-3051.

[45] Y.G. Anissimov, M.S. Roberts, Diffusion modeling of percutaneous absorption kinetics: 3. Variable diffusion and partition coefficients, consequences for stratum corneum depth profiles and desorption kinetics, J. Pharm. Sci. 93 (2004) 470-487.

[46] B. Mueller, Y.G. Anissimov, M.S. Roberts, Unexpected clobetasol propionate profile in human stratum corneum after topical application in vitro, Pharm. Res. 20 (2003) 1835-1837.

[47]S. Hansen, D. Selzer, U.F. Schaefer,G.B. Kasting, An extended database of keratin binding. J. Pharm. Sci. 100 (2011) 1712-1726.

[48] T.D. LaCount, G.B. Kasting, Human skin is permselective for the small, monovalent cations sodium and potassium but not for nickel and chromium, J. Pharm. Sci. 102 (2013) 2241-2253.

[49] P. Lai, M.S. Roberts, An analysis of solute structure-human epidermal transport relationships in epidermal iontophoresis using ionic mobility pore model, J. Control. Rel. 58 (1999) 323-333.

[50] R.O. Potts, R.H. Guy, Predicting skin permeability, Pharm. Res. 9 (1992) 663-669.

[51] G.B. Kasting, L.A. Bowman, Electrical analysis of fresh, excised human skin: a comparison with frozen skin, Pharm. Res. 7 (1990) 1141-1146.

[52] K.D. Peck, A.-H. Ghanem, W.I. Higuchi, The effect of temperature upon the permeation of polar and ionic solutes through human epidermal membrane, J. Pharm. Sci. 84 (1995) 975-982.

[53] C. Ackermann, G.L. Flynn, W.M. Smith, Ether-water partitioning and permeability through nude mouse skin in vitro. II. Hydrocortisone 21-n-alkyl esters, alkanols and hydrophilic compounds, Int. J. Pharm. 36 (1987) 67-71.

[54] A. Patzelt, J. Lademann, Drug delivery to hair follicles, Expert Opin. Drug Deliv. 10 (2013) 787-797.

[55] N. Otberg, A. Patzelt, U. Rasulev, T. Hagemeister, M. Linscheid, R. Sinkgraven, W. Sterry, J. Lademann, The role of hair follicles in the percutaneous absorption of caffeine, Brit. J. Clin. Pharmacol. 65 (2008) 488–492.

[56] S. Grimnes, Pathways of ionic flow through human skin in vivo, Acta Derm. Venereol. (Stockh.) 64 (1984) 93-98.

[57] R.R. Burnette, B. Ongpipattanakul, Characterization of the pore transport properties and tissue alteration of excised human skin during iontophoresis, J. Pharm. Sci. 77 (1988) 132-137.

[58] A. Tezel, S. Mitragotri, On the origin of size dependent tortuosity for permeation of hydrophilic solutes across the stratum corneum, J. Control. Rel. 86 (2003) 183-186.

[59] Y. Dancik, M.A. Miller, J. Jaworska, G.B. Kasting, Design and performance of a spreadsheet-based model for estimating bioavailability of chemicals from dermal exposure Adv. Drug Deliv. Rev. 65 (2013) 221-236.

[60] R. Ibrahim, J.M. Nitsche, G.B. Kasting, Dermal clearance model for epidermal bioavailability calculations, J. Pharm. Sci. 101 (2012) 2094-2108.

Graphical abstract

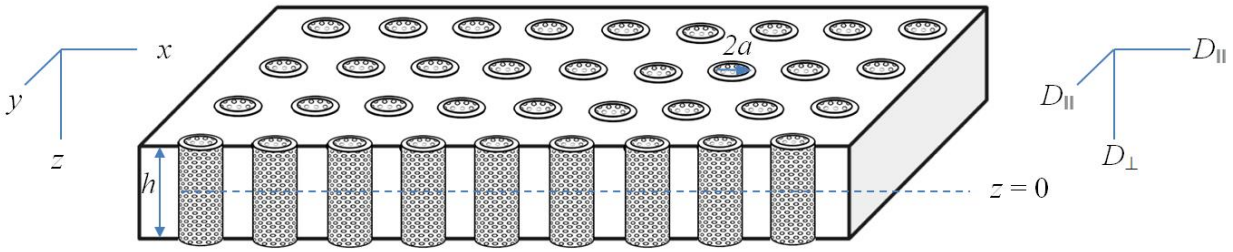

Transport of hydrophilic compounds in the stratum corneum is linked to both intracellular transport and appendageal diffusion, according to our hypothesis.